Thermal conduction in doped single-crystal silicon films

M. Asheghi[a] and K. Kurabayashi
Department of Mechanical Engineering, Stanford University, Stanford, California 94305-3030

R. Kasnavi
Department of Electrical Engineering, Stanford University, Stanford, California 94305-9505

K. E. Goodson
Department of Mechanical Engineering, Stanford University, Stanford, California 94305-3030

(Received 9 July 2001; accepted for publication 15 January 2002)

This work measures the thermal conductivities along free-standing silicon layers doped with boron and phosphorus at concentrations ranging from 1×10^{17} to 3×10^{19} cm^{-3} at temperatures between 15 and 300 K. The impurity concentrations are measured using secondary ion mass spectroscopy (SIMS) and the thermal conductivity data are interpreted using phonon transport theory accounting for scattering on impurities, free electrons, and the layer boundaries. Phonon-boundary scattering in the 3-μm-thick layers reduces the thermal conductivity of the layers at low temperatures regardless of the level of impurity concentration. The present data suggest that unintentional impurities may have strongly reduced the conductivities reported previously for bulk samples, for which impurity concentrations were determined from the electrical resistivity rather than from SIMS data. This work illustrates the combined effects of phonon interactions with impurities, free electrons, and material interfaces, which can be particularly important in semiconductor devices. © *2002 American Institute of Physics.* [DOI: 10.1063/1.1458057]

I. INTRODUCTION

Heat conduction in silicon is dominated by phonon transport, even in the presence of large concentrations of free charge carriers. The thermal conductivity of silicon layers is reduced compared to that of bulk silicon by scattering mechanisms not present in the bulk material, such as those depicted in Fig. 1. Phonon-boundary scattering is particularly important at low temperatures, where the mean free path would otherwise become arbitrarily large.[1] Also important is phonon scattering on imperfections such as vacancies and stacking faults, which are introduced during the thin-film fabrication processes. The impurities and associated free carriers in doped silicon also reduce the thermal conductivity compared to the value in bulk intrinsic silicon. The available thermal conductivity data for doped polysilicon films grown using chemical vapor deposition[2] show a reduction by more than 80% compared to those for single-crystal intrinsic silicon. This is attributed mainly to the scattering of phonons on the grain boundaries of the polysilicon films.[3]

The study of thermal conduction in doped silicon layers should begin with the existing data for bulk doped silicon.[3–6] Figures 2 and 3 present data for the bulk samples doped with phosphorus and boron together with predictions described in Sec. III B of this article. It is difficult to draw conclusions about the relative strengths of the phonon scattering mechanisms (phonon impurity, phonon electron, and phonon boundary) for four reasons. First, there are no data available for boron doped silicon samples at concentrations between 4×10^{16} and 1×10^{20} cm^{-3}. Second, the boron or phosphorus concentration was usually determined using electrical resistivity measurements. This approach is misleading when there are electrically inactive dopant atoms or unintentional impurities. Incomplete activation of boron and phosphorus is particularly important for samples doped to levels approaching the solubility limit of these impurities in silicon, which occurs at concentrations of 2×10^{20} and 1×10^{21} cm^{-3}, respectively.[7] The most common unintentional impurity in bulk silicon is oxygen, which results from the dissolution of the crucible during the Czochralski growth process.[8] Many of the samples used for thermal conductivity measurements are contaminated with oxygen.[6,9] Consequently, the reduction in thermal conductivity of these samples is due to both the impurity atoms and oxygen contamination that makes data interpretation nearly impossible. Third, the precise impact of phonon-interface scattering is difficult to assess in measurements on bulk samples. Thermal conductivity measurements for bulk silicon are usually performed on millimeter-scale samples with square or rectangular cross sections, for which the ratio of the characteristic cross-sectional dimension to the length is between 0.2 and 0.3.[4,5] This geometry renders data interpretation very difficult at low temperatures, particularly for samples with nearly specular surfaces.[10,11] The crystallographic orientation of the side faces of a sample, which are usually not specified or controlled in bulk thermal conductivity studies, can also affect the measured conductivity.[12] Fourth, the grain boundary scattering influences thermal[3] and electrical conduction[13,14] in polycrystalline samples in a manner which is difficult to assess without detailed information about the size distribution and orientation of grains. As a result, the available data for doped polycrystalline silicon films[15–17] and bulk sample[5]

[a]Present address: Mechanical Engineering Department, Carnegie Mellon University, Pittsburgh, PA 15213-3890; electronic mail: masheghi@andrew.cmu.edu

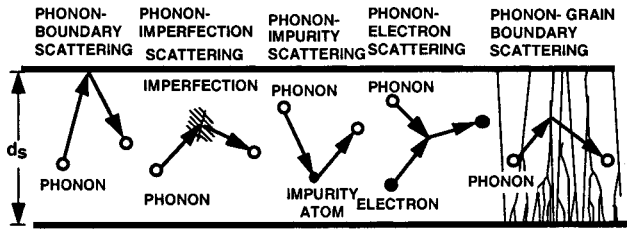

FIG. 1. Phonon scattering mechanisms that reduce the thermal conductivity of silicon regions in doped silicon layers compared to that in bulk intrinsic silicon.

(5×10^{20} boron atoms cm^{-3}) are of limited relevance for the study of heat conduction in single-crystal doped silicon layers and bulk samples.

The present work provides a systematic set of measurements of the temperature-dependent thermal conductivities of doped silicon layers. The impurity concentration is precisely determined using secondary ion mass spectroscopy (SIMS), and the layer geometry allows detailed modeling of interface scattering. The samples are free-standing silicon layers of 3 μm thickness, which are made from silicon-on-insulator (SOI) wafers. The phosphorus and boron impurity concentrations range from 1×10^{17} to 3×10^{19} cm^{-3}. The layer thermal conductivities are measured using steady-state Joule heating and electrical-resistance thermometry in patterned metal bridges. The data are interpreted using thermal conductivity modeling based on the work of Holland,[18] phonon-impurity scattering theory,[19] and phonon-electron scattering theory.[20–22]

The data and theory presented here complement the existing data for bulk samples and polycrystalline films, yielding a more comprehensive view of the impact of doping on thermal conduction in silicon. The data obtained here will assist with the thermal engineering of a broad variety of compact transistors and micromachined sensors and actuators. From a fundamental viewpoint, the data and modeling presented here provide an opportunity to study the coupled effects of phonon-boundary, phonon-impurity and phonon-electron scattering in semiconducting samples.

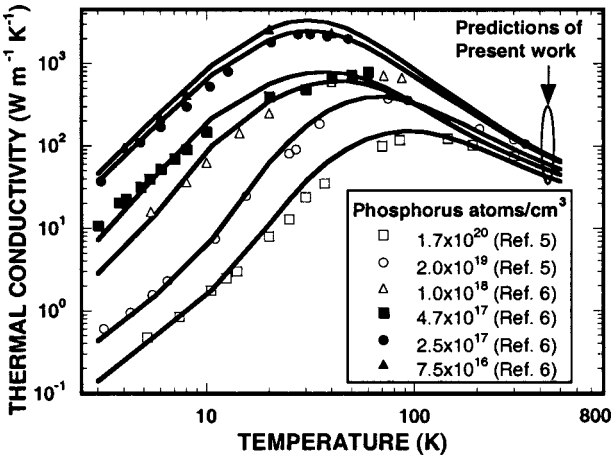

FIG. 2. Past data for the thermal conductivity of phosphorus doped silicon and predictions of the theory developed in Sec. III B to account for phonon-impurity and phonon-electron scattering in silicon.

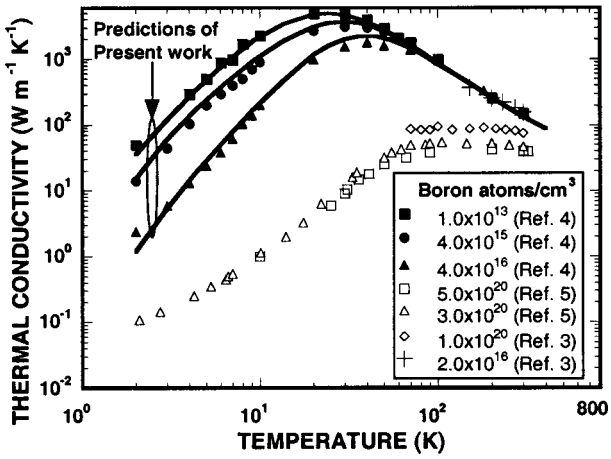

FIG. 3. Past data for the thermal conductivity of boron doped silicon and predictions of the theory developed in Sec. III B to account for the phonon-impurity and phonon-hole scattering in silicon.

II. EXPERIMENTAL STRUCTURES AND PROCEDURE

This section describes the experimental structure, fabrication process, and thermal conductivity measurement procedure for the single-crystal free-standing silicon layers. Figure 4(a) shows a top view of the experimental structure used to measure the lateral thermal conductivity of the doped silicon layers. The lateral dimensions of the suspended membrane are 1 mm×13 mm. The aluminum heater and thermometers are extended over the entire length of the membrane, but the power generated in the heater and the temperatures at points A and B are measured at the center of the suspended membrane within a region with lateral dimensions of 1 mm×1 mm. This is achieved by measuring the voltage drops in the aluminum bridges over the extent of the measurement section, L. This ensures one-dimensional heat conduction along the layer in the x direction as verified by finite element calculations. The cross-sectional schematic of the structure is shown in Fig. 4(b). The heater is located at the center of the suspended membrane. During the measurement, heat is generated by electrical current sustained in the aluminum line resulting in a linear temperature distribution along the $\langle 110\rangle$ crystallographic direction. The temperatures at two locations above the silicon layer are detected using electrical-resistance thermometry in the patterned aluminum bridges A and B.

The fabrication process for the suspended membrane is shown in Fig. 5. The starting material is a silicon-on-insulator (SOI) wafer with a 3 μm top silicon layer and 0.36 μm buried silicon dioxide layer [Fig. 5(a)], where the thin silicon layer is formed using separation by implantation of oxygen (SIMOX) technique. Thermal oxide with thickness 100 Å prevents diffusion of the dopants out of the silicon layer during the high temperature anneal. After this step, a series of ion implants are performed through the 100 Å of oxide at 180 keV to produce doped silicon layers [Fig. 5(b)]. The implants are diffused during 73 h of annealing at 1050 °C, followed by 12 h of annealing at 1150 °C to obtain a flat doping profile across the silicon layer for all concentration levels. A 3000-Å-thick layer of low temperature oxide

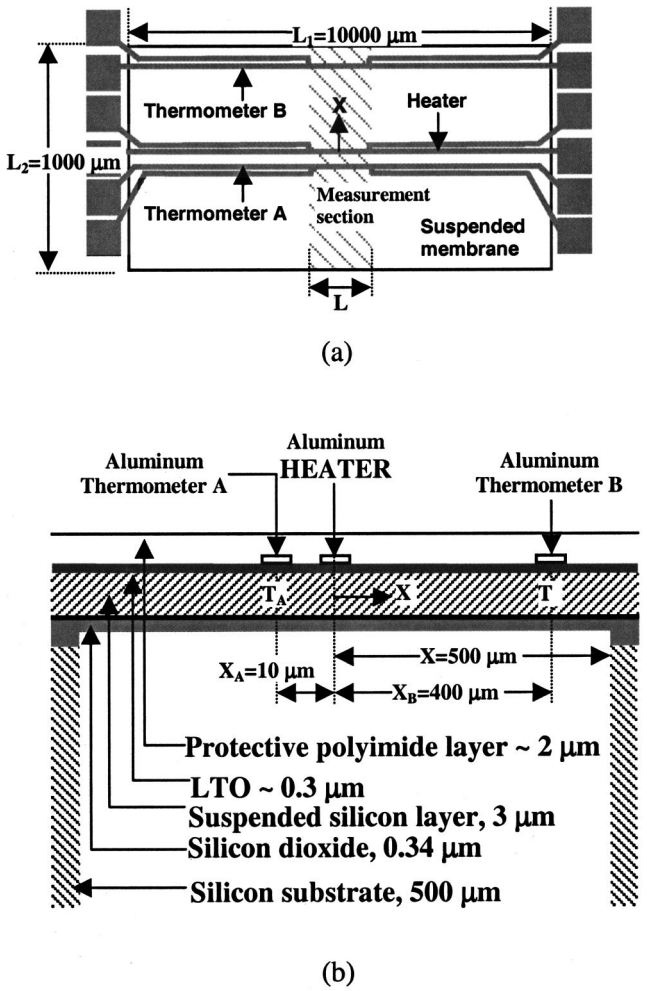

FIG. 4. (a) Top and (b) cross - sectional diagrams of the experimental structure used here to measure the lateral thermal conductivity of the SOI silicon device layer.

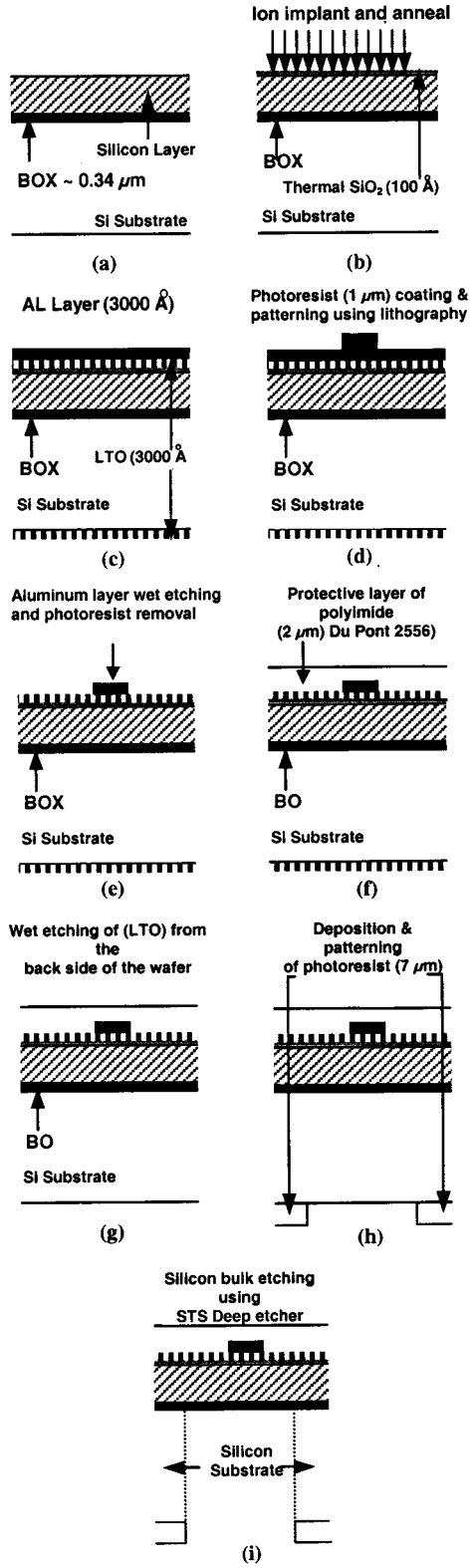

FIG. 5. Microfabrication steps for the experimental structure.

(LTO) is grown to provide electrical isolation between the doped silicon layer and the aluminum bridges, which are to be used for electrical-resistance thermometry [Fig. 5(c)]. Then 0.3-μm-thick pure aluminum is deposited and patterned (Figs. 5(c),5(d),5(e)]. A protective layer of 2-μm-thick polyimide (Dupont 2556) is spun onto the wafer and cured at 350 °C [Fig. 5(f)]. The backside LTO is then removed by wet etching using HF (6:1) [Fig. 5(g)]. The backside mask of 7-μm-thick photoresist (AZ 4620) is deposited, patterned, and baked for 45 min at 110 °C [Fig. 5(h)]. A STS deep reactive ion etching system is used to etch approximately 500 μm of silicon substrate to form a suspended membrane that consists of 3 μm silicon sandwiched between a buried oxide layer at the bottom and 3000 Å LTO and 2 μm polyimide layer at the top [Fig. 5(i)]. The concentration of impurities and uniformity of doping profiles across the 3-μm-thick silicon layers are measured using secondary ion mass spectrometry (SIMS). The nearly pure silicon layer contains less than 4×10^{14} boron, 1×10^{15} phosphorus and 4×10^{15} oxygen atoms cm^{-3}.

The heat generated at the aluminum heater is conducted predominantly along the suspended membrane in the x direction. The suspended membrane consists of four layers: the polyimide, top side LTO, silicon, and underlying silicon dioxide layers. The lateral conduction is dominated by conduction along the silicon since the thermal resistances of the polyimide, LTO, and silicon dioxide layers are at least two orders of magnitude larger than that of the silicon layer. Conduction to the surrounding air, conduction along the alumi-

num bridges, and radiation to the environment are negligible. This is established by considering the thermal resistance due to conduction along the silicon layer, $R_{\mathrm{cond,Si}} \approx (L_2/2)/2k_s d_s L$, where d_s and k_s are the thermal conductivity and thickness of the silicon layer, the width and length of the measurement section are L and L_2 [see Fig. 4(a)]. The silicon layer thermal resistance is at least two orders of magnitude less than the thermal resistance due to radiation, $R_{\mathrm{rad}} \approx \{L(L_2/2)\varepsilon\sigma[T_{\mathrm{heater}}^2 + T_{\mathrm{sur}}^2][T_{\mathrm{heater}} + T_{\mathrm{sur}}]/2\}^{-1}$. The Stefan–Boltzmann constant is $\sigma = 5.67 \times 10^{-8}$ W m^{-2} K, the emissivity ε of the silicon layer is assumed to be unity to provide an upper bound, and the heater and surrounding temperatures are T_{heater} and T_{sur}, respectively. The thermal resistance due to conduction along the silicon layer, $R_{\mathrm{cond,Si}}$, is three orders of magnitude less than the thermal resistance to conduction along the heater and thermometer legs, $R_{\mathrm{cond,Al}} \approx (L_1/2)/(12k_{\mathrm{Al}} w_{\mathrm{Al}} d_{\mathrm{Al}})$, where k_{Al}, w_{Al} and d_{Al} are the thermal conductivity, width, and thickness of a single aluminum bridge, respectively, and L_1 is the length of the suspended membrane. The measurements are performed in vacuum in order to minimize the heat conduction to the surrounding air. The thermal conductivity of the silicon layer is extracted using

$$k_s = \frac{(P/2)}{S(\Delta T/\Delta X)}, \tag{1}$$

where $P = \Delta V \times I$ is the power dissipation in the heater. The current is I and the voltage difference across the length L is ΔV. The temperature difference and separation between bridges A and B are ΔT and $\Delta X = 390$ μm. The cross-sectional area for heat conduction is $S = d_s \times L$.

The dies are attached within a 68 pin leadless chip carrier device package, wire bonded, and mounted on the chip-carrier assembly of an open-circuit cryogenic test system. The cryogenic system thermometer has an accuracy of ± 0.5 K from 10 to 100 K and 1% from 100 to 350 K. The relative uncertainties in the measurements of the power, P, and temperature difference, ΔT, are less than 1% and 0.05%, respectively. The dominant contributor to the uncertainty in the measured values of k_s is the variation in thickness of the silicon overlayer as reported by the manufacturer of the SIMOX wafers, which is nearly 10%.

III. MODELING

The thermal conductivity of the doped silicon layers is predicted using an approximate solution to the phonon Boltzmann transport equation in the relaxation time approximation together with a modified version of the Debye model for phonon specific heat. This approach was developed by Callaway[23] and refined for silicon by Holland,[18] who used a more detailed description of the phonon dispersion relations in this material to better capture the temperature dependence of the thermal conductivity. The present work modifies the model of Holland[18] to account for the increase in the phonon-scattering rate due to mass differences between the substitutional impurities and the host atom,[19] phonon-electron scattering,[20,21,24] and the small separation between the layer boundaries.[1] The appropriate scattering rates for phonon-impurity and phonon-free electrons (holes) are presented in Sec. A. Section B describes the extension of the model of Holland[18] to account for the addition of boron and phosphorus impurities. Section C accounts for the thin layer geometry.

A. Phonon scattering in doped silicon

The electrically active impurity atoms in semiconductors can strongly reduce the thermal conductivity at low temperatures.[4,5,25,26] It is widely accepted that the observed reduction in the lattice thermal conductivity with doping is due to phonon scattering on free carriers.[6,20,21,27,28] Modeling must distinguish between two categories of electron-phonon scattering: one for low concentrations, where the electron is bound to the donor impurity, and another for the high concentrations, where electrons are free to move in the conduction band. Similar argument applies to the hole-phonon scattering mechanisms. Addition of impurities to the bulk silicon results in phonon-impurity scattering due to the mass and radius differences of the impurity and host atoms.[19,29] These scattering mechanisms are discussed in the following subsections.

1. Phonon-impurity scattering

The phonon scattering on impurities, $\tau_{\mathrm{impurity}}^{-1} = \tau_{\delta M}^{-1} + \tau_{\delta R}^{-1}$ is approximated using the formula for scattering rate on point defects[19]

$$\tau_{\mathrm{impurity}}^{-1} = (A_{\delta M} + A_x)\omega^4, \tag{2}$$

where ω rad s^{-1} is the phonon angular frequency and

$$A_{\delta M} = \frac{nV^2}{4\pi v_s^3}\left(\frac{\delta M}{M}\right)^2. \tag{3}$$

The volumetric concentration of the point imperfections and the mass and crystal volume of the host atom are n, M and V, respectively. The mass difference introduced by the imperfection compared to the host atom is δM. The average velocity of sound is approximated by $v_s = \{(1/3)[v_L^{-1} + 2v_T^{-1}]\}^{-1}$, where v_L and v_T are the low frequency longitudinal and transverse phonon velocities, respectively.[18] The present work models imperfections and unintentional impurities in the doped sample using the $A_x\omega^4$ term in Eq. (2).

The insertion of the impurity atom displaces the surrounding atoms and induces strain in the lattice. The velocity of the phonons is changed by the variation in the interatomic distance, and this leads to a change in direction and a phonon scattering event. The relaxation time due to the relative displacement of the neighboring atoms, $\tau_{\delta R}$, is given by[19]

$$\tau_{\delta R}^{-1} = A_{\delta R}\omega^4, \tag{4}$$

where

$$A_{\delta R} = \frac{2nV^2}{\pi v_s^3} Q_0^2 \gamma^2 \left(\frac{\delta R}{R}\right)^2. \tag{5}$$

The Grüneisen constant, γ, is obtained from thermal expansion data[30] and the parameter Q_0 depends on how the nearest and further-out linkages combine in the scattering matrix. Typical values of $Q_0 = 4$ and 3.2 are reported for K^+ impu-

rity in NaCl and K^+ vacancy in KCl.[19] The radii of the normal ions and the difference between the radii of the foreign and normal ions are R and δR, respectively. Equation (4) is used to estimate the strength of the relaxation time due to lattice distortion.

2. Phonon-electron (hole) scattering

Ziman[20,21] studied the relaxation rate due to the scattering of phonons by electrons (holes) in metallic state. Phonon-electron interaction for the impurity states that are bound to the impurity have been considered by many researchers.[6,27,31] The transition from nonmetallic state to metallic state in semiconductors occurs when the doping concentration is higher than the transition concentration[32]

$$n_t=\left(\frac{0.25}{a_B}\right)^3, \tag{6}$$

where the effective Bohr radius is

$$a_B=\left(\frac{4\pi\varepsilon_0\hbar^2}{m_0 q_e^2}\right)\left(\frac{\varepsilon_s}{\varepsilon_0}\right)\left(\frac{m_0}{m_e}\right). \tag{7}$$

The dielectric constants in vacuum and silicon are ε_0 and ε_s, respectively, $q_e=1.6\times10^{-19}C$ is the electron charge and $\hbar=1.602\times10^{-34}$ J s is Planck's constant divided by 2π. The electron rest and effective masses are $m_0=9.11\times10^{-31}$ kg and m_e, respectively. The first term in Eq. (7) represents the Bohr radius of a hydrogen atom $=0.5$ Å and the subsequent terms are corrections due to the presence of the electron in silicon lattice. It is suggested that the transition to the metallic state for phosphorus-doped silicon should occur around 3×10^{18} cm^{-3} which has been confirmed by experimental studies of the Hall coefficient and resistivity of *n*-type silicon.[33,34] For concentrations below 2.5×10^{17} cm^{-3}, all the electrons are in the bound state.[24] The *inhomogeneity model* proposed by Mikohsiba[35] describes the electron behavior in the intermediate region for concentrations between 2.5×10^{17} and 3×10^{18} cm^{-3}. The availability of free electrons below 30 K may seem counterintuitive due to carrier freeze out. This can be explained by the overlap of the donor and conduction bands in degenerate semiconductors.[36,37]

Radhakrishnan, Sharma, and Singh[24] showed that the variation of thermal conductivity with temperature of phosphorus-doped silicon can be explained by applying the theories of phonon scattering on electrons in the localized-bound and in the metallic states. For low concentrations, the impurity forms isolated states and does not merge into the conduction band. The ground state of the donor electron in silicon is sixfold degenerate in the effective mass approximation which reflects the six equivalent conduction band minima. Degeneracy of the ground states is split into a singlet, a doublet, and a triplet due to valley-orbit interaction and central cell correction.[6] Only the elastic donor-phonon interaction between the singlet and doublet states contributes significantly to the scattering matrix.[6] The scattering rate of phonon in mode j with bound electrons, $\tau^{-1}_{j,\text{bound elec}}$, can be derived by considering the static strains as the interaction Hamiltonian[6,31]

$$\tau^{-1}_{j,\text{bound elec}}=\frac{\omega^4(0.33\Xi_{u,\text{elec}})^4}{10\pi\rho^2 v_s^2}\chi^2\left(\frac{\omega}{v_j}\right)\left\{\left[v_L^{-5}\chi^2\left(\frac{\omega}{v_L}\right)\right]+\left[v_L^{-5}\chi^2\left(\frac{\omega}{v_T}\right)\right]\right\}3w_{\text{ave}}\frac{2\Delta^2}{(\Delta^2-\hbar^2\omega^2)^2},$$
$$\left[2(n_0+n_1)+n_1\left(1+\frac{\Delta^2}{\hbar^2\omega^2}\right)\right]^2 \tag{8}$$

where $\chi(q)=[1+0.25(a_B)^2\mathbf{q}^2]^{-2}$ and $\mathbf{q}$ is the phonon wave vector. The energy difference between the singlet and doublet states is $\Delta=13$ meV and $\Xi_{u,\text{elec}}$ represents the shear deformation potential.[6] The mass density of the crystal is ρ and $w_{\text{ave}}=0.66$ represents an averaged angular weight function between the unit vectors of phonons before and after the scattering event. The number densities of electrons in the singlet and doublet states are n_0 and n_1. Since the energy difference between the singlet and doublet states are large for silicon, $n_1\approx0$, and n_0 corresponds to the number of electrons in the nonmetallic state, $n_{\text{bound,elec}}$.[6] For a given temperature, the scattering rate of the phonon-bound electron in a singlet state, Eq. (8), has three characteristic features: (a) for small frequencies, $\hbar\omega\approx\Delta$, the scattering rate is proportional to ω^4; (b) for $\hbar\omega\approx\Delta/2$ the scattering rate obeys the dependence $\tau^{-1}_{j,\text{bound elec.}}\sim\chi^4(q)$, which drops very fast as the frequency increases and serves as a cutoff factor; and (c) for $\hbar\omega\approx\Delta$, the denominator of one of the terms in Eq. (8) approaches zero resulting in a resonance behavior.

Ziman[20] obtained the phonon-free electron scattering rate for degenerate semiconductors. The elastic scattering of phonon-electron along with energy and momentum conservation laws impose a restriction on the minimum allowable wave vector of electrons, K_F, that can interact with phonons, such that $q<2K_F$. For the electrons (holes) in the metallic state, the relaxation rate due to the scattering of phonons by electrons (holes) is given by[20,21]

$$\tau^{-1}_{j,\text{free elec. (hole)}}=\frac{(m_e E_D)^2 k_B T}{2\pi\rho\hbar^4 v_j^2}\times\ln\left(\frac{1+\exp(\zeta-\zeta_0-x_\omega^2/16\zeta+x_\omega/2)}{1+\exp(\zeta-\zeta_0-x_\omega^2/16\zeta-x_\omega/2)}\right),$$
$$q<2K_F, \tag{9}$$

where

$$\zeta=\frac{m_e v_s^2}{2k_B T}. \tag{10}$$

The deformation potential is E_D, and the parameter $x_\omega=\hbar\omega/k_B T$ is the nondimensional phonon frequency where $k_B=1.38\times10^{-23}$ J K^{-1} is the Boltzmann constant. The energy difference between the Fermi level and the edge of the conduction (valence) band is ζ_0. The expression for the electron-phonon relaxation rate[20,21] approaches zero for phonon wave vectors $q<2K_F$, due to the term $x_\omega^2/16\zeta$. Equation (9) can be simplified significantly for degenerate semiconductors

$$\tau^{-1}_{j,\text{free elec. (hole)}}=\frac{(m_eE_D)^2k_BT}{2\pi\rho\hbar^4v_j^2}x_\omega, \quad q<2K_F. \tag{11}$$

It is confirmed that the Eqs. (9) and (11) are equivalent for the relevant values of $\zeta-\zeta_0$. While Eq. (9) does not explicitly depend on carrier concentration,[38] the deformation potential depends on the carrier concentration according to $E_D\propto n^{2/3}$.[39]

Kosarev[22] has shown that Eq. (9), Ziman's[20,21] expression for phonon-free electron scattering rate, cannot fully account for large reduction in the thermal conductivity of heavily doped silicon. Kosarev[22] suggested that in the presence of the electric field of ionized impurity of an atom, the phonon wave vector $q>2K_F$ can also interact with electrons. This can be considered using a relaxation rate for scattering of phonons with $q>2K_F$ represented by[22]

$$\tau^{-1}_{j,\text{free elec. (hole)}}=\frac{185n_{\text{free elec. (hole)}}(m_eE_D)^2\psi}{\rho\hbar^3q^5a_B^3} \quad q>2K_F, \tag{12}$$

where $\psi\approx1$ is the square of the cosine of the angle between the phonon wave vector $\mathbf{q}$ and the polarization e_q. Radhakrishnan, Sharma, and Singh[24] used the scattering rates for phonon-impurity and phonon-electron interactions and achieved reasonable agreement between the theory and experiments for phosphorus-doped silicon with concentrations 4.7×10^{17} and 1×10^{18} cm^{-3} at temperatures less than 30 K. The present work, however, attempts to predict the thermal conductivity of doped silicon layers for a wide range of impurity concentrations and temperature.

The elastic scattering rate due to acceptor holes in the strained crystal (lightly boron-doped silicon) is estimated using[28]

$$\tau^{-1}_{j,\text{bound hole}}=\frac{n_{\text{hole}}\omega^4(0.33\Xi_{u,\text{hole}})^4}{10\pi\rho^2v_j^2}\chi^2\left(\frac{\omega}{v_s}\right)\frac{w_j}{(\Delta^2-\hbar^2\omega^2)}\times\left\{\left[v_L^{-5}\chi^2\left(\frac{\omega}{v_L}\right)\right]+\left[v_L^{-5}\chi^2\left(\frac{\omega}{v_T}\right)\right]\right\}, \tag{13}$$

where n_{hole} and $\Xi_{u,\text{hole}}$ are the number of holes per cm^{-3} and the shear deformation potential constant for acceptor holes, respectively, and $w_L=30$ and $w_T=25$ are constant parameters.[28] The physical interpretation of the terms in Eq. (13) is similar to those of Eq. (8).

B. Thermal conductivity modeling for doped silicon

The model of Holland[18] is a refinement of the general expression for the phonon thermal conductivity[29]

$$k=\frac{1}{3}\sum_{j=L,T,TU}v_j^2\int_0^{\theta_j/T}C_{V,j}(x_\omega)\tau_j(x_\omega)dx_\omega, \tag{14}$$

where the subscripts T, TU and L indicate low and high frequency transverse and longitudinal modes, respectively. The phonon group velocity and Debye temperature of the solid are v and Θ, and C_v is the phonon specific heat per unit volume and nondimensional frequency. The three contributions to the conductivity modeled by Holland[18] differ in the value of the sound velocity and the dependence of the relaxation time on nondimensional frequency. The scattering rate in Eq. (14) is given by

$$\tau_j^{-1}=\tau^{-1}_{j,P,\text{Nb}}+\tau^{-1}_{j,P,b}, \tag{15}$$

where the subscripts P, Nb, and b refer to the nearly pure silicon, no boundary scattering and boundary scattering. The phonon relaxation time due to the boundary scattering in nearly pure silicon is $\tau_{j,P,b}=d_cF_0/v_j$. The parameter F_0 represents a correction due to both the finite length to thickness ratio of the sample and the smoothness of the surface, and the characteristic cross section of the sample is given by $d_c=2[\pi/(l_1\times l_2)]^{0.5}$, where $l_1\times l_2$ is the cross section of the bulk sample.[40] The scattering rates in the absence of phonon boundary scattering, $\tau^{-1}_{j,P,\text{Nb}}$, are given by Holland.[18]

To account for the effect of phosphorus and boron impurities, the scattering rate in Eq. (15) is modified using

$$\begin{aligned}\tau^{-1}_{j,\text{phos},B}&=\tau^{-1}_{j,P,\text{Nb}}+\tau^{-1}_{j,D,b}+\tau^{-1}_{\text{impurity}}+\tau^{-1}_{j,\text{free elec}}+\tau^{-1}_{j,\text{bound elec}},\\ \tau^{-1}_{j,\text{boron},B}&=\tau^{-1}_{j,P,\text{Nb}}+\tau^{-1}_{j,D,b}+\tau^{-1}_{\text{impurity}}+\tau^{-1}_{j,\text{free hole}}+\tau^{-1}_{j,\text{bound hole}},\end{aligned} \tag{16}$$

where the subscript B refers to the bulk silicon sample and the relaxation time, $\tau_{j,D,b}$, is due to phonon-boundary scattering in doped silicon sample. The rest of the terms are derived and discussed in Sec. III A.

C. Thermal conductivity modeling of doped silicon layers

The thermal conductivity of doped silicon layers is predicted using the model of thermal conductivity developed in Sec. III B. The relaxation time in the absence of phonon-boundary scattering in doped silicon layer is accounted for by using

$$\begin{aligned}\tau^{-1}_{j,\text{phos},B}&=\tau^{-1}_{j,P,\text{Nb}}+\tau^{-1}_{\text{impurity}}+\tau^{-1}_{j,\text{free elec}}+\tau^{-1}_{j,\text{bound elec}},\\ \tau^{-1}_{j,\text{boron},B}&=\tau^{-1}_{j,P,\text{Nb}}+\tau^{-1}_{\text{impurity}}+\tau^{-1}_{j,\text{free hole}}+\tau^{-1}_{j,\text{bound hole}},\end{aligned} \tag{17}$$

where the subscript L_y refers to the silicon layer. These expressions are different from Eq. (16) due to differences in the doping concentration and the level of unintentional impurities between the bulk sample and the thin silicon layer. The shear deformation potential constants for electrons, $\Xi_{u,\text{elec}}$, and holes, $\Xi_{u,\text{hole}}$, are adopted from the theory developed for bulk doped silicon. The relaxation time is further reduced to account for the increase in the scattering rate due to the small separation between the layer boundaries using

$$\begin{aligned}\tau_{j,\text{phos.,Ly}}&=\tau_{j,\text{phos.,Ly,Nb}}F\left(\frac{d_s}{\Lambda_{j,\text{phos,Ly,Nb}}},p\right),\\ \tau_{j,\text{boron,Ly}}&=\tau_{j,\text{boron,Ly,Nb}}F\left(\frac{d_s}{\Lambda_{j,\text{boron,Ly,Nb}}},p\right),\end{aligned} \tag{18}$$

where the boundary scattering reduction fraction F depends on the ratio of the layer thickness, d_s, and the phonon mean free path, $\Lambda_{\text{Ly,Nb}}=v\tau_{\text{Ly,Nb}}$, as well as the specular reflection

TABLE I. Parameters used to obtain agreement between the thermal conductivity data for bulk phosphorus and boron doped silicon and the theory developed. The coefficients for phonon scattering on isotopes, normal, and Umklapp processes are $A=1.32\times10^{-45}$ s^3 $B_T=9.3\times10^{-13}K^{-3}$, $B_{TU}=5.5\times10^{-18}s$, $B_L=2\times10^{-24}$ s K^{-3} (see Ref. 18).

Doping concentrations (cm^{-3})	Concentrations of electrons (holes) in metallic state, n_{free} (cm^{-3})	Concentrations of electrons (holes) in nonmetallic state, n_{bound} (cm^{-3})	Shear deformation potential, $\Xi_{u,\text{elec}}$ or $\Xi_{u,\text{hole}}$ (eV)	E_D (eV)	m_e or m_h ($/m_0$)	A_x (s^3) $\times10^{45}$
7.5×10^{16} (P)	1.88×10^{15}	7.30×10^{16}	9	0.00	0.9	0.00
2.5×10^{17} (P)	2.03×10^{16}	2.30×10^{17}	9	0.05	0.9	0.00
4.7×10^{17} (P)	6.20×10^{16}	4.08×10^{17}	9	0.22	0.9	11.75
1.0×10^{18} (P)	2.60×10^{17}	7.40×10^{17}	9	0.5	0.9	11.75
2.0×10^{19} (P)	2.00×10^{19}	2.27×10^{16}	9	1.33	0.9	5.87
1.7×10^{20} (P)	1.70×10^{20}	⋯	9	2.33	0.9	11.75
1.0×10^{13} (B)	⋯	1.00×10^{13}	4.5	0.00	0.58	0.00
4.0×10^{15} (B)	⋯	4.00×10^{15}	4.5	0.00	0.58	0.00
4.0×10^{16} (B)	1.50×10^{15}	3.85×10^{16}	4.5	0.00	0.58	0.00

coefficient p. Equation (18) uses the exact solution to the Boltzmann equation for the mean free path reduction along a thin free-standing layer[41]

$$F(\delta,p)=1-\frac{3(1-p)}{2\delta}\int_1^\infty\left(\frac{1}{t_0^3}-\frac{1}{t_0^5}\right)\times\frac{1-\exp(-\delta t_0)}{1-p\exp(-\delta t_0)}dt_0, \tag{19}$$

where the reduced thickness is $\delta=d_s/\Lambda_{\text{Ly,Nb}}$. The specular reflection coefficient can be estimated from the characteristic dimension of surface roughness, η, and the wavelength, λ, using[42]

$$p(\lambda,\eta)=\exp\left(-\frac{16\pi^3\eta^2}{\lambda^2}\right). \tag{20}$$

This approach and its implications are fully discussed by Asheghi *et al.*[1] In the present work, the model of Holland[18] is fitted to the experimental data for square cross section samples where the heat conduction occurs in the $\langle110\rangle$ crystallographic direction[12] in order to obtain the coefficients of phonon scattering rates due to isotopes, normal processes, and Umklapp processes (see the caption in Table I). The dilatation deformation potentials, E_D, the shear deformation potential, Ξ_u, and the parameters A_x and η used as fitting parameters obtain agreement between the theory and experimental data for doped silicon layers.

IV. RESULTS AND DISCUSSION

The existing thermal conductivity data for bulk doped silicon samples are examined in Sec. A and compared with the theory developed in Sec. III A. The experimental data for doped silicon layers, which is the main contribution of the present manuscript, is presented in Sec. B along with the theory developed in Sec. III B.

A. Thermal conductivity of doped bulk silicon

Figure 2 shows the previously existing thermal conductivity data for phosphorus-doped bulk silicon along with the predictions of the theory developed in this section. The thermal conductivity measurements for concentrations between 7.5×10^{16} and 1.0×10^{18} cm^{-3} were performed on crystals grown by the floating zone technique.[6] The manufacturing process of the silicon samples doped with concentrations 2.0×10^{19} and 1.7×10^{20} cm^{-3} was not specified.[5] The thermal conductivity data for lightly doped samples was fit using Eqs. (8) and (13) and the shear deformation parameter, $\Xi_{u,\text{elec}}=9$ eV, at temperatures below 20 K. The reported values in the literature are $\Xi_{u,\text{elec}}=10$ eV,[6,24] $\Xi_{u,\text{elec}}=8\pm0.3$ eV,[43] $\Xi_{u,\text{elec}}=8.6\pm0.2$ eV,[44] and $\Xi_{u,\text{elec}}=9.5$ eV.[45] The thermal conductivity data for heavily doped samples are fitted using the dilatation deformation potential, E_D (see Table I). The reported dilatation deformation potentials for nearly pure silicon are $E_{D,100}=2.4\pm0.2$ eV and $E_{D,111}=5.3\pm0.4$ eV,[44] and $E_{D,100}=2.5$ eV and $E_{D,111}=5.7$ eV,[45] where the subscript refers to a particular crystallographic direction. Quantitative comparison of the deformation potential values of the present work with those reported in the literature is relatively difficult for two reasons. First, the scattering rates in Eqs. (9) and (11) depend both on the values of effective electron mass and dilatation deformation potential. The present work assumes, $m_e=0.9m_0$, but the effective electron mass can be as small as $m_e=0.2m_0$ in a three-dimensional crystal.[46] Second, the deformation potential for doped silicon may also vary with doping concentration.[39] The effect of phosphorus impurities on the phonon-impurity scattering rate due to the mass difference and the lattice distortion is initially estimated using Eqs. (2) and (4) by assuming $A_x=0$ and $v_s=6400\ ms^{-1}$. The values $A_{\delta M}=0.23\times10^{-45}$ and $A_{\delta R}=2.66\times10^{-45}$ s^3 are obtained for a phosphorus concentration of 1.7×10^{20} cm^{-3}. These predictions, however, overestimate the data in the vicinity of the thermal conductivity maximum and at room temperature for concentrations above 1.0×10^{18} cm^{-3}. This indicates the possibility of additional imperfections in these samples.[6,24] A nominal value of $A_x=11.75\times10^{-45}$ s^3 yields reasonable agreement with the data. This coefficient is about ten times larger than the coefficients of scattering rates due to isotopes, $A_{\text{isotopes}}=1.32\times10^{-45}$ s^3, and lattice distortion, $A_{\delta R}=2.66\times10^{-45}$ s^3. It is likely that either the heavily doped samples are contaminated with oxygen atoms or that they contain a large number of

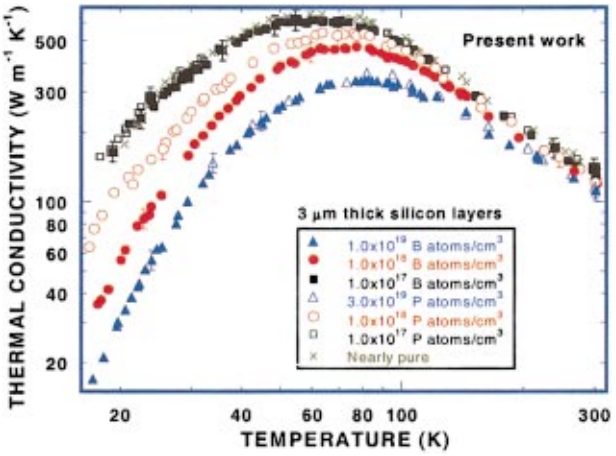

FIG. 6. (Color) Thermal conductivity data from the present study for the 3-μm-thick silicon layers.

imperfections of a different type. The predictions agree reasonably well with the data considering the complexity of the problem and wide ranges of temperature and impurity concentration. The agreement is poor for silicon doped samples with concentrations 4.7×10^{17} and 1.0×10^{18} cm^{-3} around 100 K. A similar discrepancy was observed by Fortier and Suzuki[6] and was attributed to the excessive oxygen atoms.

The thermal conductivity data for boron doped bulk silicon are reviewed in Fig. 3. The thermal conductivity data for concentrations of 1.0×10^{13}, 4×10^{15} and 4.0×10^{16} cm^{-3} were grown using the float-zone technique.[4] The data for the heavily doped samples are difficult to interpret due to the following reasons. First, the crystal growth technique for concentrations of 3.0×10^{20} and 5.0×10^{20} cm^{-3} were not specified.[5] Second, the sample with boron concentration of 5.0×10^{20} cm^{-3} is polycrystalline[5] but the grain size is not documented. Third, the level of impurities in the heavily doped samples is less certain particularly for concentrations close to the solubility limit of dopants in silicon. The resistivity measurements used to characterize these samples are more strongly influenced by the number of electrically activate impurities rather than by reflecting the full concentration of impurities. The problem is more acute for polycrystalline samples, in which the grain size can significantly alter the resistivity of the sample.[14] Fourth, the level of oxygen contamination during the silicon growth process could be as much as 40% higher for doping levels above 4.0×10^{19} cm^{-3} compared to a lightly doped crystal grown under otherwise identical conditions.[47] Under these circumstances it is not feasible to seek agreement between the theory developed here and the existing experimental data for heavily doped boron samples. The predictions for lightly boron doped silicon of concentrations 1.0×10^{13}, 4.0×10^{15} and 4.0×10^{16} cm^{-3} are based on the theory developed here. The adjustable parameters and values are given in Table I.

B. Thermal conductivity of doped silicon layers

Figure 6 shows thermal-conductivity data obtained in the present study for silicon layers as a function of temperature. The maximum in the thermal conductivity for a nearly pure 3-μm-thick silicon layer occurs near 60 K and separates the low temperature region, where scattering is dominated by imperfections and surfaces, from the high temperature region, where phonon–phonon scattering is dominant. The thermal conductivities of the silicon layers are significantly lower than the values for bulk samples due to the much stronger reduction of phonon mean free path by boundary scattering. The thermal conductivities of the silicon layers doped with boron and phosphorus at concentrations of 1.0×10^{17} cm^{-3} are nearly equal to those of the pure silicon layer, indicating that the phonon-boundary scattering dominates over the phonon-impurity scattering at low temperatures. Phonon-boundary scattering also contributes significantly to the reduction in the thermal conductivity of silicon layers regardless of the level of impurity concentration. The maximum in the conductivities for doped layers is determined by the level of impurities in the silicon layer and shifts toward higher temperatures $\approx$75 K as the impurity concentration increases. The thermal conductivities of both phosphorus and boron doped silicon layers decrease as the level of impurities increases, and the reduction is stronger for boron doped layers. The scattering rate of phonons on impurities [Eqs. (2) and (4)] is proportional to n, δM, and δR, which indicates a larger reduction in thermal conductivity for higher impurity concentrations and for greater mass and radius differences between the foreign and host atoms. This explains the stronger reduction in thermal conductivity of boron-doped compared to phosphorus-doped silicon layers given $(\delta M/M)_{\text{boron}}\approx6\times(\delta M/M)_{\text{phos}}$ and $(\delta R/R)_{\text{boron}}\approx4\times(\delta R/R)_{\text{phos}}$. The strength of phonon-impurity scattering rate ($\sim\omega^4$) diminishes at lower temperatures. The large reduction in thermal conductivity at low temperatures is generally attributed to the phonon-electron scattering in doped samples throughout the literature.[6,20–22,24]

The contribution of the oxygen atoms to the reduction in the thermal conductivity of the silicon layer is negligible for concentrations less than $\approx5\times10^{15}$ cm^{-3}.[9] The silicon layer is contaminated with less than 1×10^{11} atoms cm^{-3} of Ti, Cr, Fe, Co, Ni, Cu and Zn based on the specification of the manufacturer. The contamination level of the transition metals during the standard silicon device fabrication process does not exceed 1×10^{14} cm^{-3},[48] and it is unlikely that these impurities will reduce the thermal conductivity of silicon layers. The density of dislocations in SOI wafers is estimated[8,49] to be around 10^4-10^9 cm^{-2} which could not have possibly affected the thermal conductivity of silicon layers.

Figures 7 and 8 show the thermal conductivity data for the phosphorus and boron doped silicon layers and the predictions based on the theory developed in Sec. III C. The theory is fitted to the thermal conductivity data for nearly pure silicon layers using boundary roughness, η=2.5 Å, as an adjustable parameter at temperatures below 50 K. The value of the surface roughness is estimated to be between 2 and 10 Å for bond-and-etch-back SOI wafers[50] but should also be applicable for SIMOX wafers considering a near perfect interface between silicon and buried silicon dioxide.[8] Increasing η beyond 10 Å has a negligible effect on the

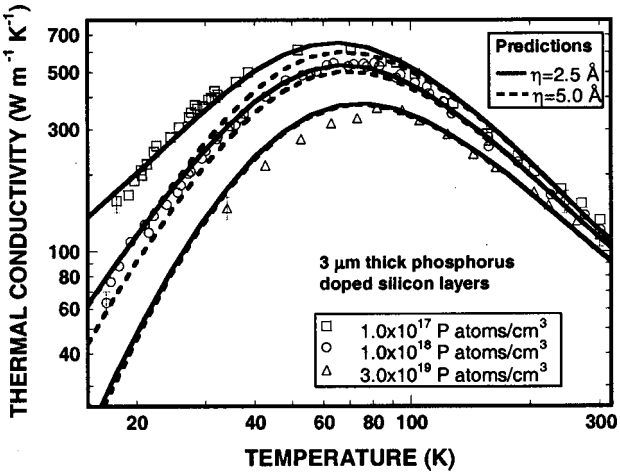

FIG. 7. Thermal conductivity data from the present study for the phosphorus doped silicon layers and the theory developed in Sec. III C.

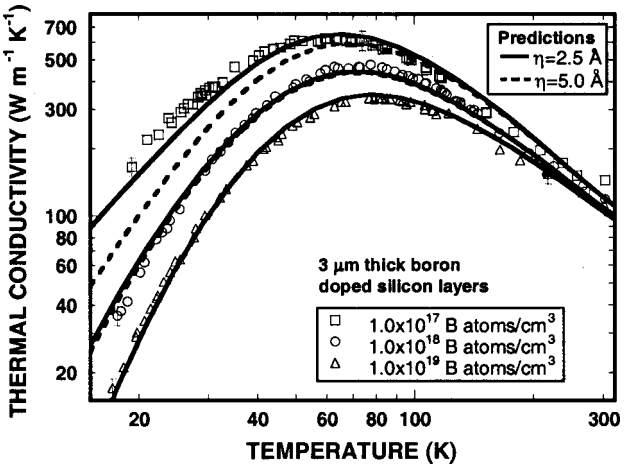

FIG. 8. Thermal conductivity data from the present study for the boron doped silicon layers and the theory developed in Sec. III C.

predicted thermal conductivity at temperatures down to 15 K.

The contributions of phosphorus and boron impurities are considered using Eq. (2) and $A_x=0$. However, the predictions slightly overestimate the thermal conductivity data around the maximum of thermal conductivity for silicon layers doped above 1.0×10^{18} cm^{-3}. The term $A_x\omega^4$ is used to evaluate the strength of the unknown scattering mechanism causing the reduction in thermal conductivity near the maxima. The values of $A_x=1.175\times10^{-45}$ and 2.35×10^{-45} s^3 are obtained for phosphorus concentrations of 1.0×10^{18} and 3.0×10^{19} cm^{-3}, respectively. Following a similar procedure, the values of $A_x=1.76\times10^{-45}$ and 2.54×10^{-45} s^3 are obtained for boron concentrations of 1.0×10^{18} and 1.0×10^{19} cm^{-3}, respectively. The effect of phonon scattering rate due to lattice distortion is estimated by Eq. (4), which yields $A_{\delta R}=0.016\times10^{-45}$ and 0.47×10^{-45} s^3 for phosphorus concentrations of 1.0×10^{18} and 3.0×10^{19} cm^{-3}, respectively. The corresponding values for boron concentrations of 1.0×10^{18} and 1.0×10^{19} cm^{-3} are $A_{\delta R}=0.25\times10^{-45}$ and 2.54×10^{-45} s^3, respectively. The values of A_x, $A_{\delta R}$, and $A_{\delta M}$ are reviewed in Table II for silicon layers with different concentrations and bulk samples doped with phosphorus up to concentration 1.0×10^{18} cm^{-3}. The strength of the scattering rates due to lattice distortion is nearly equal or on the same order of the unknown scattering rate, $A_x\omega^4$, for concentrations greater than 1.0×10^{19} cm^{-3}. It is clear that the scattering mechanism responsible for this is not very sensitive to the impurity type and roughly doubles for an order of magnitude increase in impurity concentration. The strength of the scattering rates due to lattice distortion is larger than those due to mass difference between impurity and host atom. The strength of the scattering rate due to lattice distortion for bulk phosphorus doped silicon with concentration 1.0×10^{18} cm^{-3} is one order of magnitude larger than those of the silicon layer with the same level of impurity concentration. This indicates a possibility of large contamination in bulk samples, as explained in Sec. IV A. The thermal conductivities of 3 μm silicon layers with concentrations of boron and phosphorus below 1.0×10^{17} cm^{-3} are nearly equal to those of pure silicon layers, and are strongly reduced by boundary scattering at low temperatures. The values of the adjustable parameters are given in Table III.

TABLE II. Coefficients for phonon-impurity scattering rates due to mass and radius differences between the impurity and host atoms.

Doping concentrations (cm^{-3})	$A_x\times10^{45}$ (s^3)	$A_{\delta R}\times10^{45}$ (s^3)	$A_{\delta M}\times10^{45}$ (s^3)
1.0×10^{17} (P)	0	0.0015	0.000.14
1.0×10^{18} (P)	1.17	0.015	0.0014
3.0×10^{19} (P)	2.35	0.45	0.042
1.0×10^{17} (B)	0	0.025	0.005
1.0×10^{18} (B)	1.76	0.25	0.05
1.0×10^{19} (B)	2.54	2.54	0.50
1.0×10^{18} (P) bulk	11.75	0.015	0.0014

V. SUMMARY AND CONCLUSIONS

This work uses steady-state heating and thermometry in patterned metal bridges to measure the thermal conductivity of 3-μm-thick silicon layers that have been implanted with boron and phosphorus impurities to concentrations ranging from 1×10^{17} to 3×10^{19} cm^{-3} in the temperature range 15–300 K. Secondary ion mass spectroscopy (SIMS) precisely determines the impurity concentrations. The theory applied in this manuscript separates scattering phenomena in a manner which aids with physical interpretation of the data. The thermal conductivities of 3 μm silicon layers with concentrations of boron and phosphorus below 1×10^{17} cm^{-3} are nearly equal to those of pure silicon layers, and are strongly reduced by boundary scattering at low temperatures. The thermal conductivities of silicon layers doped with boron are lower than those of the layers doped with phosphorus impurity, which is consistent with the different rates of phonon scattering on these impurities. The phonon-boundary scattering also contributes significantly to the reduction in the thermal conductivity of silicon layers regardless of the level of impurity concentration except for highest impurity concentration levels (3×10^{19} cm^{-3} for phosphorus and 1×10^{19}

TABLE III. The values of the adjustable parameters for the thermal conductivity predictions of Figs. 7 and 8.

Impurity concentrations (cm^{-3})	Concentrations of electrons (holes) in metallic state, n_{free} (cm^{-3})	Concentrations of electrons (holes) in nonmetallic state, n_{bound} (cm^{-3})	Shear deformation potential, $\Xi_{u,elec}$ or $\Xi_{u,hole}$ (eV)	E_D (eV)	m_e or m_h ($/m_0$)	A_x (s^3) $\times 10^{45}$
1.0×10^{17} (P)	6.2×10^{16}	4.08×10^{17}	9	0.16	0.9	0
1.0×10^{18} (P)	2.6×10^{17}	7.40×10^{17}	9	0.5	0.9	1.17
3.0×10^{19} (P)	3.0×10^{19}	2.27×10^{16}	9	1.33	0.9	2.35
1.0×10^{17} (B)	6.2×10^{16}	4.08×10^{17}	4.5	0.16	0.58	0
1.0×10^{18} (B)	2.6×10^{17}	7.40×10^{17}	4.5	4	0.58	1.76
1.0×10^{19} (B)	1.0×10^{19}	2.00×10^{16}	4.5	5	0.58	2.54

cm^{-3} for boron) at temperatures below 20 K. The data provided in this manuscript are valuable for fundamental studies of phonon-boundary, phonon-impurity and phonon-electron scattering mechanisms. Comparison between the experimental data and theory for doped silicon layer shows that the expressions for phonon scattering rates due to mass and radius difference between the impurity and host atoms may not be adequate to explain the variation in thermal conductivity with temperature and impurity concentration. It is concluded that a large fraction of the reduction in thermal conductivity of bulk doped silicon samples may have been due to contamination of samples by oxygen atoms and unintentional impurities.

ACKNOWLEDGMENTS

This work was sponsored by Semiconductor Research Corporation (SRC) under Contract No. 98-PJ-461. This work made use of the National Nanofabrication Users Network facilities funded by the National Science Foundation under Award No. ECS-9731294. Mehdi Asheghi appreciates assistance from Eugene Chow in the fabrication of the experimental structure.

[1] M. Asheghi, M. N. Touzelbaev, K. E. Goodson, Y. K. Leung, and S. S. Wong, J. Heat Transfer **120**, 30 (1998).
[2] Y. C. Tai, C. H. Mastrangelo, and R. S. Muller, J. Appl. Phys. **65**, 1442 (1988).
[3] M. Asheghi, Ph.D. thesis, Stanford University, 1999.
[4] G. Holland and L. J. Neuringer, in *Proceedings of the International Conference on the Physics of Semiconductors*, Exeter (The Institute of Physics and Physical Society, London, 1962), p. 474.
[5] G. Slack, J. Appl. Phys. **35**, 3460 (1964).
[6] D. Fortier and K. Suzuki, J. Phys. (Paris) **37**, 143 (1976).
[7] R. B. Fair, Electrochemical Society Spring Meeting, Philadelphia, PA, May 1977, p. 1027.
[8] S. M. Sze, *VLSI Technology* (McGraw-Hill, New York, 1998).
[9] G. S. Verma, Phys. Rev. B **18**, 5903 (1978).
[10] T. Klitsner, J. E. VanCleve, H. E. Fischer, and R. O. Pohl, Phys. Rev. B **38**, 7576 (1988).
[11] M. Asen-Palmer, K. Bartkowski, E. Gmelin, M. Cardona, A. P. Zhemov, A. V. Inyushkin, A. Taldenkov, V. L. Ozhogin, K. M. Itoh, and E. E. Haller, Phys. Rev. B **56**, 9431 (1997).
[12] A. K. McCurdy, H. J. Maris, and C. Elbaum, Phys. Rev. B **2**, 4077 (1970).
[13] K. E. Goodson, J. Heat Transfer **118**, 279 (1996).
[14] L. Gerzberg, N. C. C. Lu, and J. D. Meindl, IEEE Electron Device Lett. **1**, 38 (1980).
[15] F. Volklein and H. Baltes, J. Microelectromech. Syst. **1**, 193 (1992).
[16] C. H. Mastrangelo and R. S. Muller, Sens. Mater. **3**, 133 (1988).
[17] M. Von Arx, O. M. Paul, and H. Baltes, Sens. Actuators A **47**, 428 (1995).
[18] M. G. Holland, Phys. Rev. **132**, 2461 (1963).
[19] P. G. Klemens, Proc. Phys. Soc., London **68**, 1113 (1955).
[20] J. M. Ziman, Philos. Mag. **1**, 191 (1955).
[21] J. M. Ziman, Philos. Mag. **2**, 292 (1957).
[22] V. V. Kosarev, Sov. Phys. JETP **33**, 793 (1971).
[23] J. Callaway, Phys. Rev. **113**, 1046 (1959).
[24] V. Radhakrishnan, P. C. Sharma, and M. Singh, Z. Phys. B **39**, 15 (1980).
[25] S. S. Devlin, *Transport Properties in Physical and Chemistry of II-IV Compounds*, edited by M. Aven and J. S. Prener (North-Holland, Amsterdam, 1967).
[26] D. M. Rowe and C. M. Bandhari, Prog. Cryst. Growth Charact. **13**, 233 (1980).
[27] A. Griffin and P. Carruthers, Phys. Rev. **131**, 1976 (1963).
[28] K. Suzuki and N. Mikoshiba, J. Phys. Soc. Jpn. **31**, 44 (1971).
[29] R. Berman, *Thermal Conduction in Solids* (Oxford University Press, Oxford, UK, 1976).
[30] G. Slack and S. F. Bartram, J. Appl. Phys. **46**, 89 (1975).
[31] R. W. Keyes, Phys. Rev. **122**, 1171 (1961).
[32] N. F. Mott, Phys. Rev. **113**, 147 (1956).
[33] M. N. Alexander and D. F. Hocomb, Rev. Mod. Phys. **40**, 815 (1968).
[34] C. Yamanouchi, K. Mizuguchi, and W. Sasaki, J. Phys. Soc. Jpn. **22**, 859 (1967).
[35] N. Mikoshiba, Rev. Mod. Phys. **40**, 833 (1968).
[36] D. S. Lee and G. J. Fossum, IEEE Trans. Electron Devices **30**, 626 (1983).
[37] A. H. Marshak and C. M. Van Vliet, Proc. IEEE **72**, 148 (1984).
[38] G. P. Srivastava, *The Physics of Phonons* (Hilger, Bristol, 1990).
[39] M. J. Ziman, *Electrons and Phonons* (Oxford University Press, Oxford, United Kingdom, 1960).
[40] H. B. G. Casimir, Physica (Utrecht) **5**, 495 (1938).
[41] E. H. Sondheimer, Adv. Phys. **1**, 1 (1952).
[42] R. Berman, E. L. Foster, and J. M. Ziman, Proc. R. Soc. London, Ser. A **231**, 130 (1955).
[43] J. E. Aubrey, W. Gubler, T. Henningsen, and H. Koenig, Phys. Rev. **130**, 1667 (1963).
[44] I. Balslev, Phys. Rev. **143**, 636 (1966).
[45] I. Goroff and L. Kleinman, Phys. Rev. **132**, 1080 (1963).
[46] H. D. Barber, Solid-State Electron. **10**, 1039 (1967).
[47] C. W. Pearce, R. J. Jaccodine, A. J. Filo, and W. Lin, Appl. Phys. Lett. **46**, 887 (1985).
[48] P. F. Schmidt and C. W. Pearce, J. Electrochem. Soc. **128**, 630 (1981).
[49] D. I. Ma, J. G. Campisi, S. B. Qadri, and M. C. Peckerar, Thin Solid Films **206**, 27 (1991).
[50] W. P. Maszara, J. Electrochem. Soc. **138**, 341 (1991).